Journal of the American Heart Association

ORIGINAL RESEARCH

Integrin α7 Mutations Are Associated With Adult-Onset Cardiac Dysfunction in Humans and Mice

Enrico Bugiardini, MD, PhD*; Andreia M. Nunes, PhD*; Ariany Oliveira-Santos, MSc*; Marisela Dagda, MSc; Tatiana M. Fontelonga, PhD; Pamela Barraza-Flores, PhD; Alan M. Pittman, PhD; Jasper M. Morrow, PhD; Matthew Parton, MD; Henry Houlden, PhD; Perry M. Elliott, MD; Petros Syrris, PhD; Roderick P. Maas, MD; Mohammed M. Akhtar, MD; Benno Küsters, MD, PhD; Joost Raaphorst, MD, PhD; Meyke Schouten, MD; Erik-Jan Kamsteeg, PhD; Baziel van Engelen, MD, PhD; Michael G. Hanna, MD; Rahul Phadke, MD; Luis R. Lopes, MD, PhD; Emma Matthews, MD; Dean J. Burkin, PhD

BACKGROUND: Integrin α7β1 is a major laminin receptor in skeletal and cardiac muscle. In skeletal muscle, integrin α7β1 plays an important role during muscle development and has been described as an important modifier of skeletal muscle diseases. The integrin α7β1 is also highly expressed in the heart, but its precise role in cardiac function is unknown. Mutations in the integrin α7 gene (*ITGA7*) have been reported in children with congenital myopathy.

METHODS AND RESULTS: In this study, we described skeletal and cardiac muscle pathology in *Itga7*$^{-/-}$ mice and 5 patients from 2 unrelated families with *ITGA7* mutations. Proband in family 1 presented a homozygous c.806_818del [p.S269fs] variant, and proband in family 2 was identified with 2 intron variants in the *ITGA7* gene. The complete absence of the integrin α7 protein in muscle supports the *ITGA7* mutations are pathogenic. We performed electrocardiography, echocardiography, or cardiac magnetic resonance imaging, and histological biopsy analyses in patients with *ITGA7* deficiency and *Itga7*$^{-/-}$ mice. The patients exhibited cardiac dysrhythmia and dysfunction from the third decade of life and late-onset respiratory insufficiency, but with relatively mild limb muscle involvement. Mice demonstrated corresponding abnormalities in cardiac conduction and contraction as well as diaphragm muscle fibrosis.

CONCLUSIONS: Our data suggest that loss of integrin α7 causes a novel form of adult-onset cardiac dysfunction indicating a critical role for the integrin α7β1 in normal cardiac function and highlights the need for long-term cardiac monitoring in patients with *ITGA7*-related congenital myopathy.

Key Words: cardiomyopathy ■ congenital muscular dystrophy ■ congenital myopathy ■ integrin α7

Integrins are heterodimeric cell receptors composed of α- and β-subunits that act as cell mechanosensors and mechanotransducers. Integrins serve as a transmembrane linkage system that binds extracellular matrix proteins to the cortical actin inside the cell.[1–4] The integrin α7β1 is a major laminin receptor and regulator of skeletal muscle development and disease. In skeletal muscle, integrin α7β1 is localized throughout the myofiber and enriched at myotendinous and neuromuscular junctions, where it plays a

Correspondence to: Dean J. Burkin, PhD, Department of Pharmacology, University of Nevada, Reno School of Medicine, Reno, NV 89557.
Email: dburkin@med.unr.edu
Emma Matthews, MBChB, MD, The Atkinson Morley Neuromuscular Centre and Regional Neurosciences Centre, St George's University Hospitals NHS Foundation Trust; and Molecular and Clinical Sciences Research Institute, St George's University of London, London, UK.
Email: e.matthews@sgul.ac.uk
*E. Bugiardini, A. M. Nunes, and A. Oliveira-Santos contributed equally.

Supplemental Material is available at https://www.ahajournals.org/doi/suppl/10.1161/JAHA.122.026494
For Sources of Funding and Disclosures, see page 11.

JAHA is available at: www.ahajournals.org/journal/jaha

CLINICAL PERSPECTIVE

What Is New?

- This study identifies 5 new patients from 2 families with integrin α7 deficiency that exhibit a novel form of adult-onset cardiac dysfunction.
- The adult-onset cardiac dysfunction is mainly characterized by first-degree heart block and intraventricular conduction delay.
- To our knowledge, this study characterizes for the first time a mouse model that recapitulates human integrin α7 (*ITGA7*) gene-related cardiac disease and supports the use of this preclinical model to investigate the mechanistic role of integrin α7 in cardiac function.

What Are the Clinical Implications?

- The present study highlights the requirement for long-term cardiac monitoring in patients with *ITGA7*-related congenital myopathy.
- Our study supports genetic screening for mutations in the *ITGA7* gene for patients who present with myopathy of unknown genetic cause.

Nonstandard Abbreviations and Acronyms

Cx43	connexin-43
ITGA7	integrin subunit alpha 7 (Human gene)
Itga7	integrin subunit alpha 7 (Mouse gene)
WT	wild-type

critical role during neuromuscular and myotendinous junctions development, myoblast migration, and myofiber survival.[5–15] Integrin α7β1 is also expressed in satellite cells and differentiating myoblasts and serves as an important regulator of muscle regeneration and repair.[5,8,9,16,17] Several isoforms of integrin α7 are generated by alternative RNA splicing.[18–20] Integrin α7A and α7B cytoplasmic variants are the major isoforms in human skeletal muscle,[9] whereas the α7B isoform is the only one found in cardiomyocytes.[21] Integrin α7X1 and α7X2 extracellular isoforms have been shown to bind with different affinities to various laminin isoforms.[22]

The integrin α7β1 is detected during late fetal mouse cardiac development and in adult cardiac muscle.[9,21,23–25] The integrin α7β1 is a major modifier in muscular dystrophy,[10,12] and mutations in the integrin α7 (*ITGA7*) gene, which encodes the integrin α7 protein, cause congenital myopathy. Some studies have described skeletal muscle pathology or dysfunction in patients and mice lacking integrin α7, but these only involved a limited number of patients with *ITGA7* deficiency with pediatric clinical presentations.[26–31] Only 1 study has reported a proband carrying variants in *ITGA7* and *MYH7* (myosin heavy chain beta) genes with features of cardiomyopathy.[29] Other family members demonstrating isolated cardiomyopathy only carried the *MYH7* variant, and therefore the role of integrin α7 in cardiac function remains unknown.

Here, we report mutations in the integrin α7 gene are associated with adult-onset cardiac dysfunction in humans and mice. This study uncovers an important role for integrin α7 in normal cardiac function and identified integrin α7-related cardiac arrhythmia as a novel form of cardiac dysfunction.

METHODS

The data that support the findings of this study are available from the corresponding author upon reasonable request.

Next Generation Sequencing

Family 1, II.4 was screened using the SureSelect Focused Exome (Agilent) kit, according to the manufacturer's protocol. Sequencing was performed on a Hiseq 1500 (Illumina, CA). The Illumina fastq sequencing data were mapped to the human reference assembly, hg19 (GRCh37; University of California, Santa Cruz genome browser) by Novoalign Software (Novocraft Inc). After removal of polymerase chain reaction duplicates (Picard) and reads without a unique mapping location, variants were extracted using the Maq model in SAMtools and outputted by the following criteria: consensus quality >30, single nucleotide polymorphism quality >30, and root mean square mapping quality >30. These variant calls were then annotated using Annovar software. Variants with an allele frequency higher than 1% in ExAC, 1000 Genome, or ESP6500 database were filtered out. Synonymous and deep intronic variants were excluded from the analysis. We screened and analyzed 322 genes related to neuromuscular disease and hereditary cardiomyopathies reported in the GeneTable of Neuromuscular Disorders.[32]

Family 2, II.4 was screened using SureSelectXT Human All Exon 50 Mb Kit V5 (Agilent). Sequencing was performed using a Hiseq 4000 (Illumina). Read mapping and variant calling were conducted using Burrows-Wheeler Aligner software package BWA (http://bio-bwa.sourceforge.net/index.shtml) and the genome analysis toolkit GATK (https://software.broadinstitute.org/gatk/; Broad Institute, Cambridge), respectively. Annotation of variants was done using in-house pipelines and a muscle disease gene panel was applied (Genome Diagnostics, Radboudumc & Maastricht University Medical Center, The Netherlands). Additional screening of genes (n=21) associated with

hypertrophic cardiomyopathy was performed. Variants with an allele frequency higher than 1% in gnomAD / ExAC or higher than 1% in the Radboudumc exome database of >50 000 control exomes were filtered out. Deep intronic variants were excluded from the analysis (standard settings of the "variant effect predictor" from the ensemble).

Mice Genotyping

Itga7$^{-/-}$ mice were generated and genotyped as previously described.[33] Heterozygous *Itga7* mice were crossed to obtain homozygous *Itga7*$^{-/-}$ mutants and C57BL/6J wild-type (WT) control littermates. Mice were euthanized by CO_2 asphyxiation followed by cervical dislocation under the American Veterinary Medical Association guidelines for euthanasia. For this study, a total of 17 *Itga7*$^{-/-}$ mice and 15 WT littermates were used.

Isolation of Cardiac Myocytes

Single ventricular myocytes were isolated from adult Hartley guinea pigs as described previously.[34] The methods followed *The Guide for the Care and Use of Laboratory Animals*, as adopted by the National Institutes of Health and approved by the Institutional Animal Care and Use Committee at the University of Nevada, Reno.

Immunofluorescence

Cryosections from human and murine muscle biopsies were incubated with primary antibodies. Human muscle biopsies were incubated for 1 hour at room temperature with the following primary antibodies: integrin α7 (1:400, Abcam Ab75224), integrin α5 (1:80, Abcam Ab6131), integrin β1D (1:100, Abcam Ab8991), laminin α2-1 (300kDa) (1:50, Alexis 804-190-C100), laminin α2-2 (80kDa) (1:4000, Millipore MAB1922), and laminin α5 (1:4000, Millipore MAB1924). Murine muscle sections were incubated overnight at 4 °C with the following primary antibodies: integrin α7B,[20] integrin β1D,[20] laminin (pan antibody against skeletal muscle laminin isoforms) (Sigma L9393; 1:400), laminin α2 (Sigma L0663; 1:100), and connexin-43 ([Cx43] Thermo Fisher Scientific CX-1B1; 1:200). The sections were then washed using 0.1 M PBS pH 7.2. Human muscle biopsy sections were incubated with biotinylated secondary antibodies (1:200) for 30 minutes at room temperature. After washing with PBS, the human muscle biopsy sections were incubated with streptavidin-conjugated to Alexa Fluor 594 (1:1000, Molecular Probes) for 15 minutes at room temperature. Following another wash, human muscle sections were mounted using Hydromount mounting medium. In parallel, murine muscle sections were incubated with secondary antibodies conjugated with fluorescein isothiocyanate and tetramethylrhodamine (Jackson Immuno Research, 1:200) for 1 hour at room temperature and mounted with Vectashield Antifade Mounting Medium with 4′,6-diamidino-2-phenylindole. Imaging for human muscle biopsies was performed on a Leica DM6B epifluorescent microscope, whereas images from murine muscle specimens were acquired on an Olympus IX81 microscope. The acquired images were analyzed in Fiji version 1.49.

Histology

Sirius Red staining was performed on murine muscle sections. Sections were hydrated in a series of 100%, 95%, and 80% ethanol gradient incubations of 3 minutes each. The sections were then washed in water and stained with Gills Hematoxylin (S5400-1D, Fisher Scientific) for 10 minutes. After washing, the sections were incubated in Scott solution for 3 minutes, washed once again, and incubated in 0.1% Sirius Red/Picric Acid (SO-674, Rowley Biochemical) for 30 minutes. The sections were then washed twice for 5 minutes in acidified water and dehydrated in a series of 80%, 95%, and 100% ethanol gradient incubations for 10 minutes each. The dehydration was followed by a 5-minute incubation with Xylene and mounting with dibutylphthalate polystyrene xylene DEPEX medium.

Electrocardiography

Electrocardiography was performed as validated.[35] 10-month-old *Itga7*$^{-/-}$ mice (n=8) and wild-type littermates (C57BL/6J) (n=10) were anesthetized with 2% isoflurane mixed with 0.5 L/min 100% O_2 and kept on a heating pad to maintain constant body temperature. Three shielded lead wire electrodes (AD Instruments, Australia) were inserted subcutaneously. Lead II tracings were recorded using PowerLab 6/26 supplemented with an animal Dual BioAmp and analyzed with LabChart Pro software (AD Instruments). Lead II channel was amplified and sampled at a rate of 4 kHz and 5 mV range of a high-pass filter setting of 1 Hz. Averaged electrocardiography parameters were obtained from continuous 10-minute recordings.

Echocardiography

Transthoracic echocardiography was performed on 10-month-old *Itga7*$^{-/-}$ mice (n=12) and WT littermates (C57BL/6J) (n=12) following published guidelines.[36] Mice were anesthetized with 2% isoflurane mixed with 0.5 L/min 100% O_2 and kept on a heating pad to maintain body temperature. Scanning was performed using the Vevo2100 image system with a high-resolution transducer at a frequency of 40 MHz (MS550) (FUJIFILM VisualSonics, Canada). Two-dimensional B-mode images and left ventricular M-mode tracings

were acquired from the parasternal short-axis view at the papillary muscles level. M-mode measurements were analyzed using Vevo LAB v3.2.0 (FUJIFILM VisualSonics).

Study Approval

The human study was conducted in accordance with the Declaration of Helsinki. Informed consent for genetic research testing was obtained from all patients where applicable and the study was performed with institutional ethical approval. Family 1 was evaluated at the Queen Square Centre for Neuromuscular Diseases, National Hospital for Neurology and Neurosurgery, and at the Barts Heart Centre, London, UK. Family 2 was assessed at the Department of Neurology, Radboud University Medical Center, Nijmegen, The Netherlands.

All procedures involving mice were performed under the approved protocol 00399 from the Institutional Animal Care and Use Committee of the University of Nevada, Reno.

Statistical Analysis

All data are expressed as mean ± SEM. All measurements followed the normal distribution. Student *t*-test was performed on WT versus *Itga7*$^{-/-}$ values for electrocardiography and echocardiography data using GraphPad Prism software. Representative *P* values and symbols are described in the figure legends.

RESULTS

We identified 5 individuals from 2 unrelated families (Figure 1A and 1B) with a clinical presentation of adult-onset cardiac conduction defects, respiratory insufficiency, and mild skeletal myopathy (Table S1). The proband in family 1 is a 52-year-old man from Kashmir (Figure 1A; II.4). Next generation sequencing identified a homozygous c.806_818del [p.S269fs] variant in *ITGA7* (NM_002206.3) that was confirmed by Sanger sequencing (Figure S1). The variant is extremely rare in the general population (0.000004 in Gnomad v2.1.1) with no homozygous case reported. No alternative or concomitant relevant pathogenic variant in other genes was found. Aside from isolated stridor at birth because of vocal cord paresis, early history was unremarkable. He presented with palpitations, first-degree heart block (PR interval 200 ms), intraventricular conduction delay, and left axis deviation at age 37 years (data not shown). By the age of 47 years, the PR interval on his ECG had progressed to 222 ms and QRS duration to 136 ms with intraventricular conduction delay (Figure 1Ca). Further investigation revealed paroxysmal atrial flutter that was successfully treated by ablation. Subsequent 24-hour Holter analysis identified frequent ventricular ectopy (>3000 PVC/24 hours) including runs of nonsustained ventricular tachycardia, as well as intermittent episodes of Mobitz type 1 second-degree atrioventricular block. Transthoracic echocardiography and cardiac magnetic resonance imaging demonstrated localized left ventricular hypertrophy confined to the basal-mid inferior wall (maximal wall thickness 15 mm) with preserved left ventricular systolic function (Figure 1Cb and 1Ce). Computed tomography coronary angiography was normal. Given the presence of progressive conduction disease, together with evidence of nonsustained ventricular tachycardia and new symptoms of presyncope, the patient received an implantable cardioverter-defibrillator. Cardiac assessment of an elder brother (Figure 1A; II.3) revealed similar cardiac pathology with conduction abnormalities, mild left ventricular hypertrophy, and limited fibrosis (see Table S1 and Figure S2). Quadriceps muscle histopathology was consistent with a mild myopathy (Table S1). Respiratory insufficiency with nocturnal hypoventilation and chronic respiratory acidosis requiring bilevel positive airway pressure therapy was evident from his early 50s (Table S1).

Next generation sequencing in the proband from family 2 (Figure 1B; II.4) identified 2 intron variants in the *ITGA7* gene (NM_002206.3) (c.2357+1G>A [r.spl?] and c.2278-1G>A [r.spl?]) affecting canonical splicing sites. These variants are extremely rare in the general population (MAF 0.000035 and no cases reported, respectively) with no homozygous cases reported. No alternative or concomitant relevant pathogenic variant in other genes was found. The presence of these variants was confirmed by Sanger sequencing (Figure S1), and the complete absence of integrin α7 staining in the muscle supports that both mutations are pathogenic and likely in trans position (Figure 2G). She was hospitalized at age 61 years with a history of relapsing respiratory insufficiency of unknown cause from her early 50s. Medical history was notable for cataract, left bundle branch block, atrial flutter, and high-grade atrioventricular block necessitating implantation of a dual-chamber rate-modulated pacemaker. Aside from a pCO_2 of 10.87 kPa, the neuromuscular examination was unremarkable with only mild bilateral weakness of ankle dorsiflexion (Medical Research Council score 4+). Ascites were present on the systemic examination. Investigations including quadriceps muscle biopsy were indicative of a myopathic disorder (Table S1). Family history revealed that a sister (Figure 1B; II-7), who had right ventricular failure, pulmonary hypertension, and restrictive pulmonary disease of unknown cause, had died of respiratory insufficiency at age 55 years. Another sister (II-8) was assessed at the age of 46 for limb-girdle muscular weakness and respiratory failure postoperatively. Following genetic analysis in the proband, the same *ITGA7* variants were identified in her affected siblings (Figure 1B).

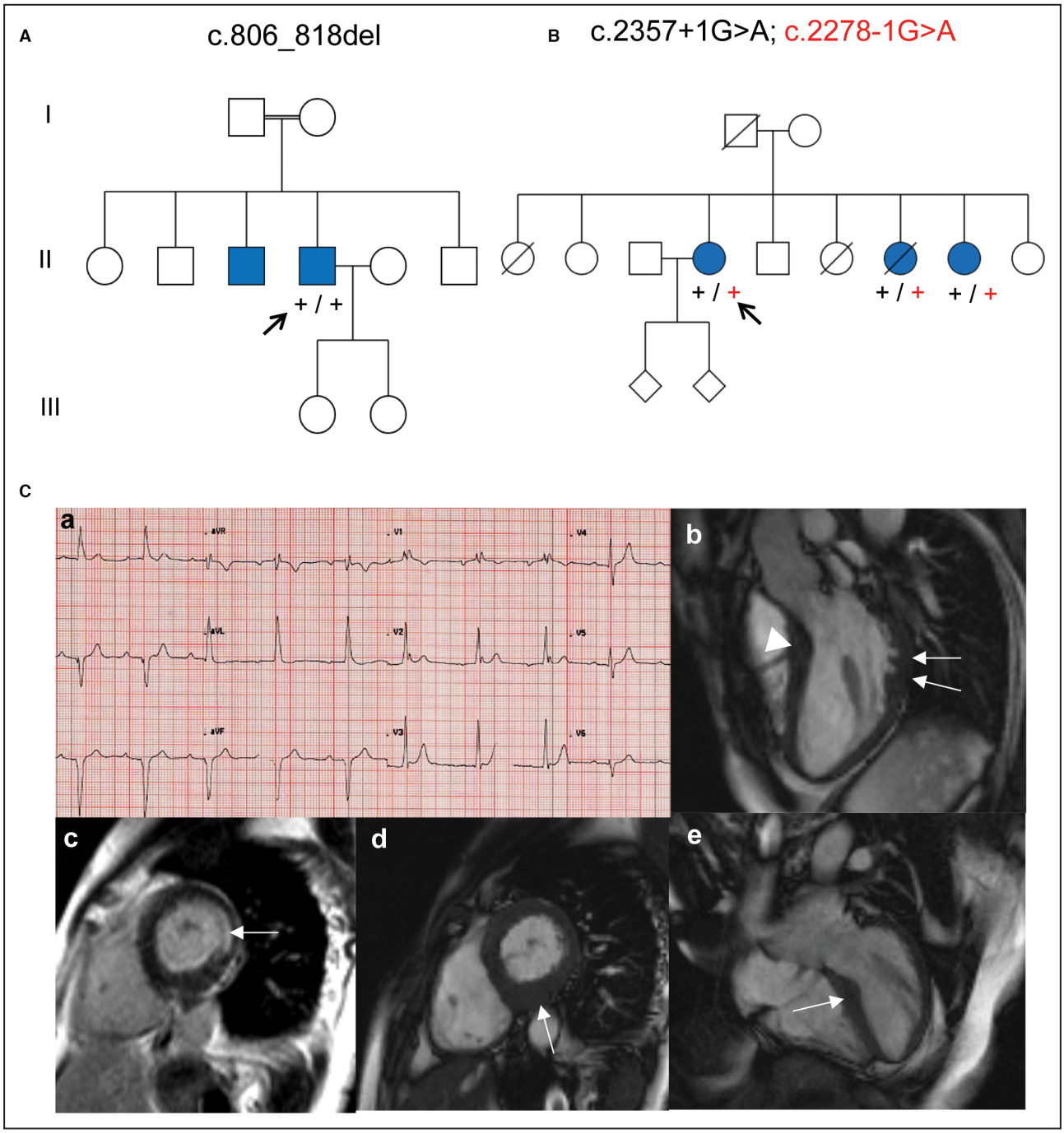

Figure 1. Patient family pedigree and respective cardiac investigation.
Pedigree of families 1 and 2 (**A** and **B**) with filled blue shapes representing affected family members. In (**A**), arrow indicates the family 1 proband (A-II:4), and the black plus signs (+) indicate the identified alleles c.806_818del variant in integrin α7 gene (NM_002206.3). In (**B**), arrow indicates the family 2 proband (B-II:4), the black plus signs indicate the alleles c.2357+1G>A and red plus signs indicate the alleles c.2278-1G>A variants in integrin α7 gene identified in the genetically tested family members. Electrocardiography in family 1 proband (II:4) demonstrated first-degree heart block, intraventricular conduction delay, left axis deviation, and PR interval 222 ms and QRS duration 136 ms (**Ca**). Cardiac magnetic resonance imaging, 3 chamber cine, end-diastole, showing basal septal mild hypertrophy (white arrowhead) and 3 basal inferolateral crypts (white arrows) (**Cb**). Cardiac magnetic resonance imaging, basal short-axis late gadolinium enhancement image showing fibrosis in the inferolateral wall (white arrow) (**Cc**). Cardiac magnetic resonance imaging, basal short-axis cine, end-diastole, showing localized hypertrophy in the basal inferior wall (white arrow) (**Cd**). Cardiac magnetic resonance imaging, 4 chamber cine, end-diastole, revealing mild basal septal hypertrophy (white arrow) (**Ce**).

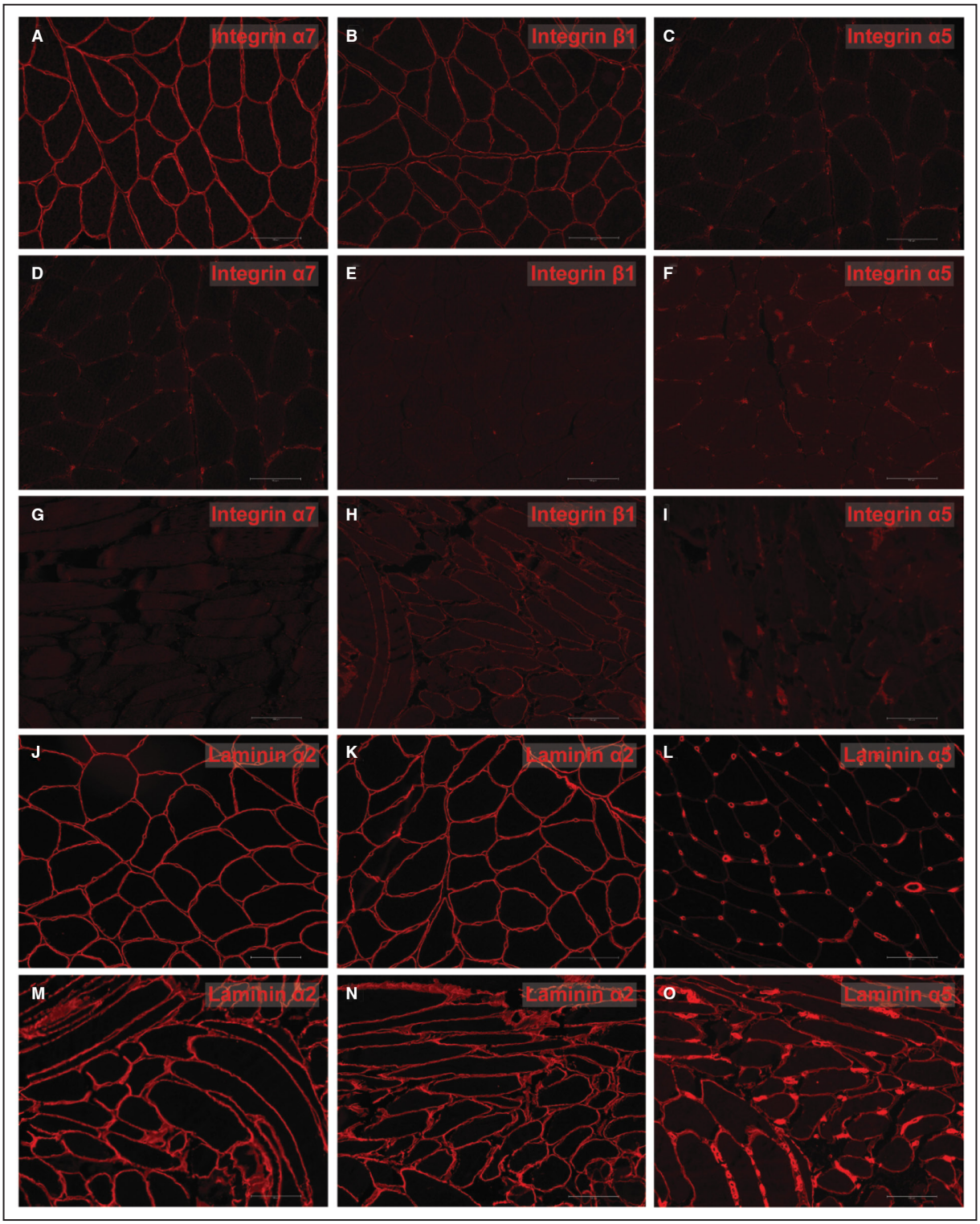

Figure 2. Myopathy in patients with integrin α7 gene deficiency.
Quadriceps muscle biopsies from the family 1 proband taken at 37 years (**D** through **F**), the family 2 proband (**G** through **I**, **M** through **O**) taken at 62 years, and an unaffected adult control (**A** through **C**, **J** through **L**). Immunofluorescent staining of frozen sections is shown for integrin α7 (**A**, **D,** and **G**), integrin β1D (**B**, **E,** and **H**), integrin α5 (**C**, **F,** and **I**), laminin α2 with 2 different antibodies (**J**, **M**, **K,** and **N**), and laminin α5 (**L** and **O**). There is a complete absence of integrin α7 (**D** and **G**) and a reduction of integrin β1D (**E** and **H**) at the sarcolemma in both patients compared with the control (**A** and **B**). Integrin α5 staining is present on endomysial capillaries (**F** and **I**) comparable to the control (**C**). In the family 2 proband, immunostaining for laminin α2 (**M** and **N**) is comparable with the control (**J** and **K**), and there is also considerable upregulation of laminin α5 (**O**) at the basal lamina compared with the normal endomysial vascular labeling in the control (**L**). Scale bar: 100 μm.

To characterize the myopathic disorder in more detail, we reanalyzed quadriceps muscle biopsies from the 2 probands and an unaffected adult control muscle biopsy by immunofluorescence (Figure 2). We detected an absence of sarcolemmal localized integrin α7 in both probands' biopsies (Figure 2D and 2G) compared with the unaffected adult control (Figure 2A) and a reduction of integrin β1D in both probands' biopsies (Figure 2E and 2H) compared with the unaffected adult control (Figure 2B). Integrin α5 expression was seen in the endomysial capillaries of both patients' biopsies (Figure 2F and 2I) similar to the adult control (Figure 2C). Laminin α2 expression in the family 2 proband biopsy (Figure 2M and 2N) was comparable with the adult control (Figure 2J and 2K). Laminin α5 expression was restricted to the endomysial vasculature in the adult control (Figure 2L) but secondarily upregulated on the myofiber basal lamina in the family 2 proband biopsy (Figure 2O).

We next analyzed muscles from the *Itga7*$^{-/-}$ mouse model (19). Analysis of 8-month-old *Itga7*$^{-/-}$ mice diaphragm muscle revealed a decrease in integrin β1D (Figure S3E), but no change in laminin α2 (Figure S3F) compared with WT controls (Figure S3A and S3B). Laminin α5 was upregulated in the diaphragm of *Itga7*$^{-/-}$ mice (Figure S3G) compared with WT controls (Figure S3C), but no significant changes in laminin α2 or α5 were observed in the gastrocnemius muscle of *Itga7*$^{-/-}$ mice (Figure S3M and S3N) compared with WT controls (Figure S3I and S3J), suggesting that changes in laminin α5 protein in the diaphragm muscle may serve as a compensatory mechanism.

We also analyzed the fibrotic content in skeletal muscle of *Itga7*$^{-/-}$ mice. We detected increased fibrosis in the diaphragm (Figure S3H) and gastrocnemius (Figure S3O and S3P) muscles of *Itga7*$^{-/-}$ mice compared with WT (Figure S3D, S3K and S3L). Whereas the collagen content was increased throughout the diaphragm (Figure S3H), *Itga7*$^{-/-}$ gastrocnemius muscle exhibited only a few fibrotic regions (Figure S3O and S3P), indicating the diaphragm is more affected in 8-month-old mice.

We next characterized electrical and mechanical cardiac function in *Itga7*$^{-/-}$ mice. Abnormal electrocardiography patterns and mechanical function were detected at 10 months of age in *Itga7*$^{-/-}$ hearts (Figures 3 and 4). Lead II electrocardiography analysis showed a significant increase in PR, QRS, and QT intervals in *Itga7*$^{-/-}$ mice compared with WT (Figure 3F through 3H). We also observed increased P duration in *Itga7*$^{-/-}$ mice (Figure 3E). In the cardiac cycle, we found a decrease in R amplitude in *Itga7*$^{-/-}$ murine hearts compared with WT hearts (Figure 3K), while no significant differences in P, Q, S, and T amplitudes, heart rate, and RR interval were detected (Figure 3I, 3J, 3L, 3M, 3C, and 3D).

Mechanical cardiac function parameters were significantly reduced in 10-month-old *Itga7*$^{-/-}$ mice compared with age-matched WT controls. *Itga7*$^{-/-}$ mice presented reduced ejection fraction, fractional shortening, cardiac output, and stroke volume (Figure 4D through 4G). We also observed a 14% increase in the left ventricular posterior wall thickness at diastole (Figure 4K) and a decrease of about 20% in the left ventricular anterior wall thickness at systole (Figure 4N) in *Itga7*$^{-/-}$ mice compared with WT controls. No significant differences between the 2 groups were observed in the other parameters analyzed (Figure 4C, 4H, 4I, 4J, 4L, 4M, and 4O).

To further elucidate the role of integrin α7 in cardiac function, WT and *Itga7*$^{-/-}$ murine cardiac muscle sections were immunolabeled for integrin α7B, α5, α6, β1D, laminin α2, and Cx43 (Figure S4). While integrin α7B is absent in *Itga7*$^{-/-}$ hearts, as revealed by immunohistochemistry, in the ventricle anterior wall (Figure S4F) and in the compact ventricle myocardium (Figure S4N), we did not detect major differences in integrin β1D expression (Figure S4G) when compared with WT controls (Figure S4B, S4J, and S4C). Integrin α5 was localized to the intercalated discs and integrin α6 was localized to the lateral membrane of *Itga7*$^{-/-}$ hearts (Figure S4O and S4P) similar to WT hearts (Figure S4K and S4L). The absence of integrin α7 did not affect the expression of laminin-α2 (Figure S4E and S4I), β-dystroglycan (Figure S4M and S4Q), talin (Figure S5A and S5C), or vinculin (Figure S5B and S5D).

Cx43 (connexin-43) is widely expressed in the heart and can be found in the lower brand branches, Purkinje fibers, and atrial and ventricular cardiomyocytes.[37] We confirmed Cx43 protein localization at gap junctions in adult WT mouse cardiac muscle (Figure 5A through 5E) and cardiomyocytes isolated from the guinea pig (Figure S6A through S6D) where it colocalizes with integrin α7 at the intercalated discs of cardiomyocytes. We also detected Cx43 in *Itga7*$^{-/-}$ Purkinje fibers (Figure S4D and S4H). Interestingly, we identified Cx43 redistribution to the lateral membrane in *Itga7*$^{-/-}$ cardiomyocytes (Figure 5F through 5J). Additionally, histological qualitative analysis of fibrosis in *Itga7*$^{-/-}$ mice revealed no difference in the fibrotic content between the hearts of WT (Figure 5K and 5K') and *Itga7*$^{-/-}$ mice (Figure 5L and 5L').

DISCUSSION

We report that *ITGA7* mutations that result in loss of integrin α7 protein might cause adult-onset cardiomyopathy with cardiac conduction defects and mechanical dysfunction, respiratory insufficiency, and myopathic features. Our data show that loss of integrin α7 in mice leads to myopathy with predominant diaphragmatic involvement resembling the clinical features observed in the patients. The lack of integrin α7 also results in cardiomyopathy with cardiac conduction defects and mechanical dysfunction in *Itga7*$^{-/-}$ mice that resemble

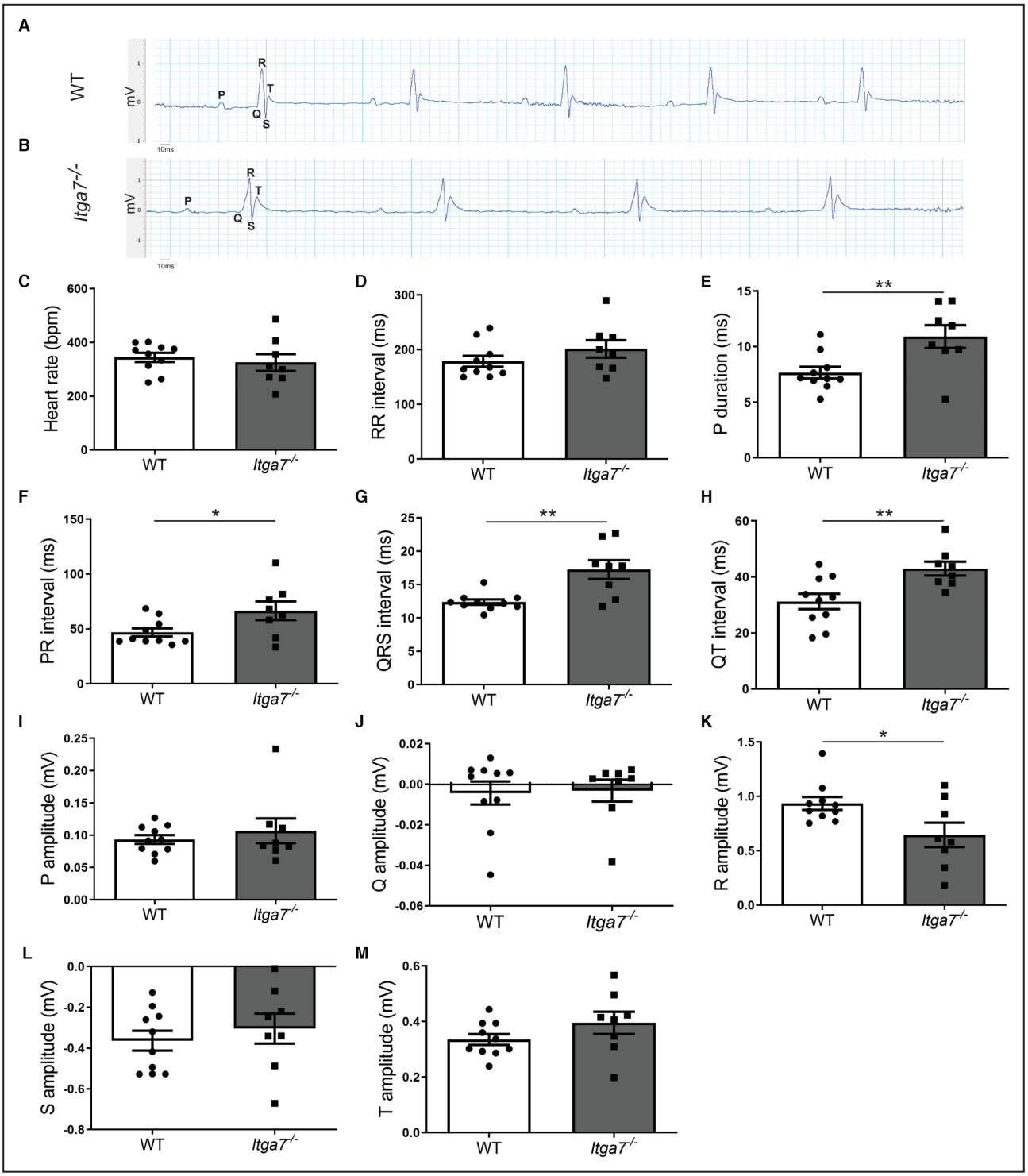

Figure 3. Electrocardiography analysis in wild-type and *Itga7*$^{-/-}$ mice.
Representative traces are shown from a lead II ECG from 10-month-old wild-type (n=10) (**A**) and *Itga7*$^{-/-}$ mice (n=8) (**B**). Quantitative evaluation reveals prolonged P duration (**E**) and PR interval (**F**) suggesting alterations in conduction through the atrioventricular node, and prolonged QRS interval (**G**) and QT interval (**H**) in *Itga7*$^{-/-}$ mice indicating ventricular conduction delay. No significant difference was found in heart rate (**C**), RR interval (**D**), P amplitude (**I**), Q amplitude (**J**), S amplitude (**L**), and T amplitude (**M**). In the absence of integrin α7, R amplitude (**K**) is significantly decreased. Student *t*-test analysis represented by statistical significance of mean±SEM.*P<0.05, **P<0.01. *Itga7*$^{-/-}$, indicates integrin α7 knockout; and WT, wild-type.

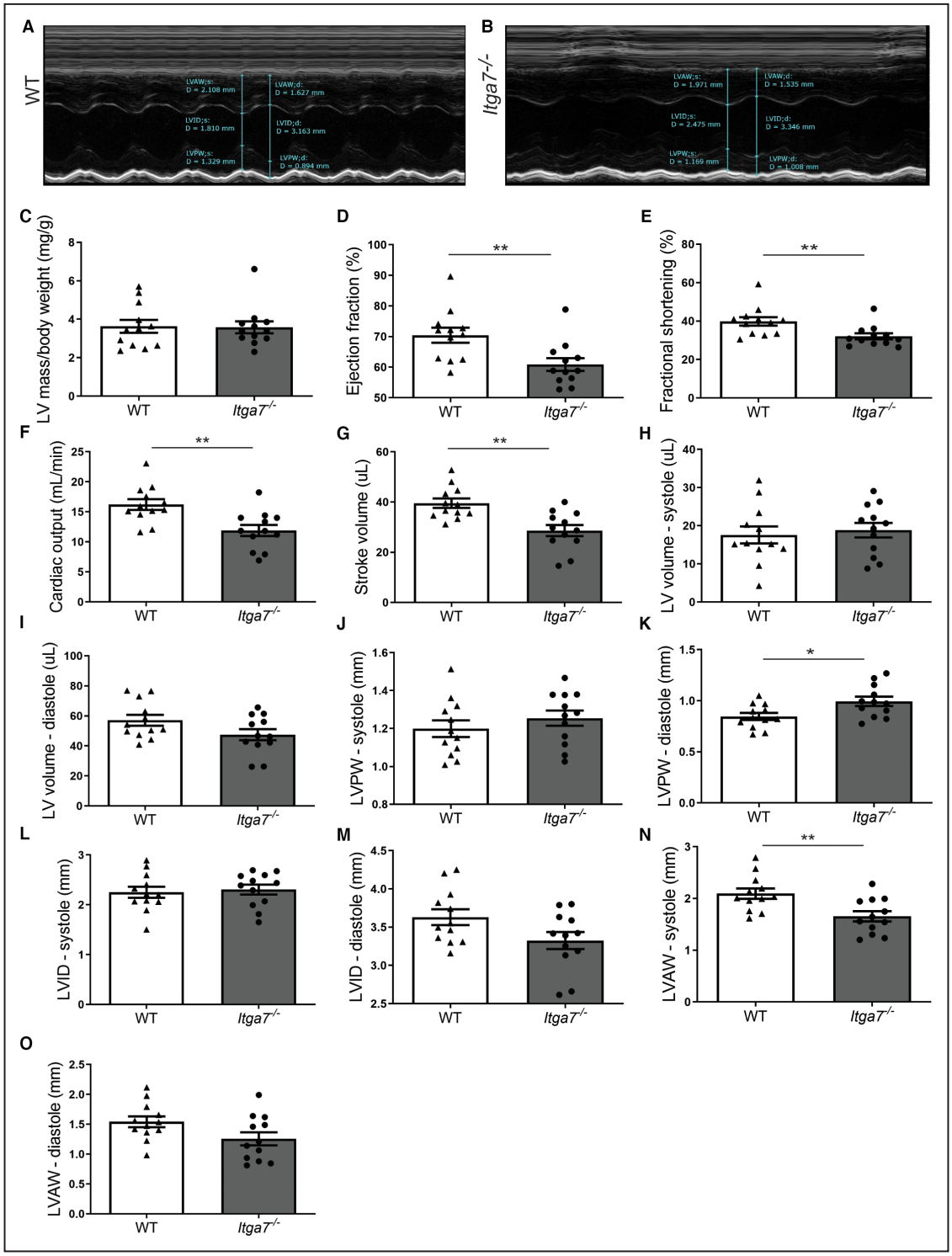

Figure 4. Echocardiography analysis in wild-type and *Itga7*$^{-/-}$ mice.
Representative echocardiograms (M-mode view) of 10-month-old wild-type (n=12) (**A**) and *Itga7*$^{-/-}$ mice (n=12) (**B**). Echocardiographic measurements show reduced ejection fraction (**D**), fractional shortening (**E**), cardiac output (**F**), and stroke volume (**G**) in *Itga7*$^{-/-}$ mice suggesting systolic dysfunction. No significant differences were found in left ventricular (LV) mass/body weight ratio (**C**), LV systolic volume (**H**), LV diastolic volume (**I**), LV posterior wall thickness at systole (**J**), LV internal diameter at systole (**L**), LV internal diameter at diastole (**M**), and LV anterior wall thickness at diastole (**O**). *Itga7*$^{-/-}$ mice presented a significant increase of about 14% in LV posterior wall thickness at diastole (**K**) and a decrease of about 20% in LV anterior wall thickness at systole (**N**). Student *t*-test analysis represented by statistical significance of mean ± SEM.*P<0.05, **P<0.01. d indicates diastole; *Itga7*$^{-/-}$, integrin α7 knockout; LV, left ventricle; LVAW, left ventricular anterior wall; LVID, left ventricular internal diameter; LVPW, left ventricular posterior wall; and WT, wild-type.

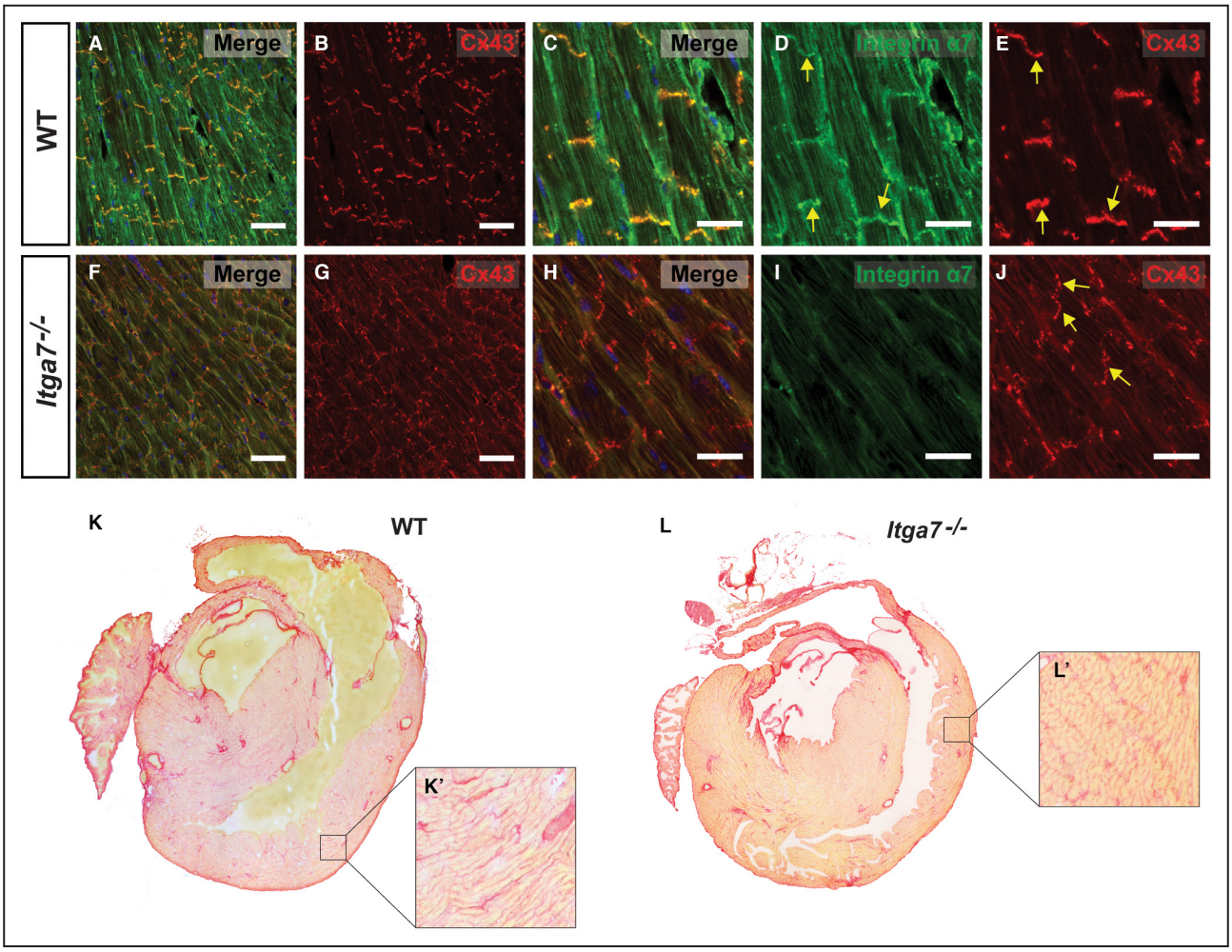

Figure 5. Histological analysis of wild-type and *Itga7*$^{-/-}$ cardiac muscle.
Transversal view of immunostaining for integrin α7 (green) (**A**, **C**, **D**, **F**, **H**, and **I**) and connexin-43 (red) (**A**, **B**, **C**, **E**, **F**, **G**, **H**, and **J**) in wild-type (A-E) and *Itga7*$^{-/-}$ (**F** through **J**) cardiac muscle. Connexin-43 localization is restricted to the intercalated discs in wild-type cardiomyocytes (**A**, **B**, **C**, and **E**), whereas connexin-43 is redistributed to the lateral membrane of the *Itga7*$^{-/-}$ (**F**, **G**, **H**, and **J**) cardiomyocytes. Sirius Red staining for wild-type (**K** and **K′**) and *Itga7*$^{-/-}$ (**L** and **L'**) cardiac muscle reveals no significant changes in fibrosis levels in the absence of integrin α7. Yellow arrows indicate positive staining for integrin α7 (**D**) and connexin-43 (**E** and **J**). The merge images include 4'6-diamidino-2-phenylindole (blue), integrin α7 (green), and connexin-43 (red). Cx43 indicates connexin-43; *Itga7*$^{-/-}$, integrin α7 knockout; and WT, wild-type. Representative images of n=3 for each genotype. Scale bar: 25 μm.

the probands who presented first-degree heart block and intraventricular conduction delay.

We also identified the importance of integrin α7β1 in the localization of Cx43 in murine cardiomyocytes which when altered could contribute to the pathological mechanism of *ITGA7*-related cardiac arrhythmias and systolic dysfunction. Cx43 is an important component of gap-junction channels located at the intercalated discs where it mediates cardiomyocyte contraction by regulating intercellular ion propagation in cardiac muscle.[38–40] Interestingly, Cx43 redistribution to the lateral membrane of cardiomyocytes has been shown to contribute to altered cardiac electrical conduction, arrhythmias, and reduced contractile function of the heart.[41] Cx43 remodeling has also been associated with many cardiac diseases including Duchenne muscular dystrophy-related arrhythmogenesis,[42,43] hypertrophic cardiomyopathy, and heart failure.[44] Altered electrical conduction and reduced systolic function observed in *Itga7*$^{-/-}$ mice may be related to the Cx43 remodeling observed in *Itga7*$^{-/-}$ cardiomyocytes. Taken together, our results suggest that Cx43 redistribution might be associated with the mechanosensing and mechanotransduction function of integrin α7 in cardiac muscle.

Another possible consequence of the loss of *ITGA7* may include impaired L-type calcium channel activity involved in ventricle depolarization.[45] This was previously shown to be regulated by laminin and integrin β1 interactions in cat atrial myocytes.[46] Kwon et al. have also found that integrin α7β1 regulates voltage-gated L-type calcium channels in myogenic cells through laminin-binding or integrin α7 activating antibodies.[47]

Moreover, studies have shown integrin α7 interacts with and stabilizes RyR2 (ryanodine receptor 2) to protect cardiomyocytes from ischemia/reperfusion injury.[48] Further studies will be needed to elucidate if any of these mechanisms also contribute to the altered cardiac electrical activity observed in patients with *ITGA7*-deficiency and *Itga7*$^{-/-}$ mice.

Together, this study identifies a potential novel role for the integrin α7β1 in normal cardiac function and indicates a potential new genetic cause for idiopathic adult-onset cardiac dysfunction. Our study also highlights the need for long-term cardiac monitoring in patients with *ITGA7*-related congenital myopathy. Finally, our study supports genetic screening for mutations in the *ITGA7* gene for patients who present with myopathy and predominant respiratory involvement.

ARTICLE INFORMATION

Received April 18, 2022; accepted November 2, 2022.

Affiliations

Queen Square Centre for Neuromuscular Diseases, Queen Square Institute of Neurology, UCL and National Hospital for Neurology and Neurosurgery, London, United Kingdom (E.B., J.M.M., M.P., M.G.H.); Department of Pharmacology, University of Nevada Reno, School of Medicine, Center for Molecular Medicine, Reno, NV (A.M.N., A.O., M.D., T.M.F., P.B., D.J.B.); Department of Neuromuscular Diseases, UCL Queen Square Institute of Neurology, London, United Kingdom (A.M.P., H.H.); St George's, University of London, London, United Kingdom (A.M.P.); Barts Heart Centre, Barts Health NHS Trust, London, United Kingdom (P.M.E., M.M.A., L.R.L.); Centre for Heart Muscle Disease, Institute of Cardiovascular Science, University College London, London, United Kingdom (P.M.E., P.S., M.M.A., L.R.L.); Department of Neurology, Donders Institute for Brain, Cognition and Behaviour (R.P.M., B.v.E.); and Department of Pathology (B.K.), Radboud University Medical Center, Nijmegen, The Netherlands; Department of Neurology, Amsterdam University Medical Centre, University of Amsterdam, Amsterdam Neuroscience, Amsterdam, The Netherlands (J.R.); Department of Human Genetics, Radboud University Medical Center, Nijmegen, The Netherlands (M.S., E.K.); Division of Neuropathology, UCL Institute of Neurology, London, United Kingdom (R.P.); Dubowitz Neuromuscular Centre, MRC Centre for Neuromuscular Diseases, UCL Great Ormond Street Institute of Child Health, London, United Kingdom (R.P.); The Atkinson Morley Neuromuscular Centre and Regional Neurosciences Centre, St George's University Hospitals NHS Foundation Trust, London, United Kingdom (E.M.); and Molecular and Clinical Sciences Research Institute, St George's University of London, London, United Kingdom (E.M.).

Acknowledgments

The authors would like to thank Dr Arie van Dijk, cardiologist, and Dr Yvonne Heijdra, pulmonologist, both at the Radboud University Medical Center, Nijmegen, the Netherlands, for providing clinical data.

Sources of Funding

This study was supported by grants from the Muscular Dystrophy Association (MDA238981 and MDA628561) and National Insitutes of Health - National Institute of Arthritis and Musculoskeletal and Skin Diseases (NIH-NIAMS) (R01AR064338; R01AR053697) to D. Burkin. A. Oliveira-Santos was supported by a Raymond H. Berner Graduate School Scholarship. T. Fontelonga was supported by a Mick Hitchcock Scholarship. Dr Phadke was supported by National Health Service (NHS) England Highly Specialised Service for Congenital Myopathies and Congenital Muscular Distrophies. Dr Matthews was supported by a Wellcome Clinical Research Career Development Fellowship. Dr Lopes was supported by a Medical Research Council UK Clinical Academic Research Partnership award. Part of this work was undertaken at University College London Hospitals/University College London, which received a proportion of funding from the Department of Health's National Institute for Health Research Biomedical Research Centres funding scheme.

Disclosures

The authors have declared that no conflict of interest exists.

Supplemental Material

Table S1
Figures S1–S6

REFERENCES

1. Hynes RO. Integrins: bidirectional, allosteric signaling machines. *Cell.* 2002;110:673–687. doi: 10.1016/S0092-8674(02)00971-6
2. Ingber DE. Mechanical control of tissue morphogenesis during embryological development. *Int J Dev Biol.* 2006;50:255–266. doi: 10.1387/ijdb.052044di
3. Barczyk M, Carracedo S, Gullberg D. Integrins. *Cell Tissue Res.* 2010;339:269–280. doi: 10.1007/s00441-009-0834-6
4. Takada Y, Ye X, Simon S. The integrins. *Genome Biol.* 2007;8:215. doi: 10.1186/gb-2007-8-5-215
5. Echtermeyer F, Schöber S, Pöschl E, Von Der Mark H, Von Der Mark K. Specific induction of cell motility on laminin by α7 integrin. *J Biol Chem.* 1996;271:2071–2075. doi: 10.1074/jbc.271.4.2071
6. Yao CC, Ziober BL, Squillace RM, Kramer RH. α7 integrin mediates cell adhesion and migration on specific laminin isoforms. *J Biol Chem.* 1996;271:25598–25603. doi: 10.1074/jbc.271.41.25598
7. Crawley S, Farrell EM, Wang W, Gu M, Huang HY, Huynh V, Hodges BL, Cooper DNW, Kaufman SJ. The α7β1 integrin mediates adhesion and migration of skeletal myoblasts on laminin. *Exp Cell Res.* 1997;235:274–286. doi: 10.1006/excr.1997.3671
8. Vachon PH, Xu H, Liu L, Loechel F, Hayashi Y, Arahata K, Reed JC, Wewer UM, Engvall E. Integrins (a7b1) in muscle function and survival. *J Clin Invest.* 1997;100:1870–1881. doi: 10.1172/JCI119716
9. Burkin DJ, Kaufman SJ. The alpha7beta1 integrin in muscle development and disease. *Cell Tissue Res.* 1999;296:183–190. doi: 10.1007/s004410051279
10. Hodges BL, Hayashi YK, Nonaka I, Wang W, Arahata K, Kaufman SJ. Altered expression of the alpha7beta1 integrin in human and murine muscular dystrophies. *J Cell Sci.* 1997;110:2873–2881. doi: 10.1242/jcs.110.22.2873
11. Cohn RD, Mayer U, Saher G, Herrmann R, Van Der Flier A, Sonnenberg A, Sorokin L, Voit T. Secondary reduction of α7B integrin in laminin α2 deficient congenital muscular dystrophy supports an additional transmembrane link in skeletal muscle. *J Neurol Sci.* 1999;163:140–152. doi: 10.1016/S0022-510X(99)00012-X
12. Doe J, Wuebbles RD, Allred ET, Rooney JE, Elorza M, Burkin DJ. Transgenic overexpression of the α7 integrin reduces muscle pathology and improves viability in the dy(W) mouse model of merosin-deficient congenital muscular dystrophy type 1A. *J Cell Sci.* 2011;124:2287–2297. doi: 10.1242/jcs.083311
13. Laprise P, Vallee K, Demers MJ, Bouchard V, Poirier EM, Vezina A, Reed JC, Rivard N, Vachon PH. Merosin (laminin-2/4)-driven survival signaling: complex modulations of Bcl-2 homologs. *J Cell Biochem.* 2003;89:1115–1125. doi: 10.1002/jcb.10581
14. Baudoin C, Goumans MJ, Mummery C, Sonnenberg A. Knockout and knockin of the β1 exon D define distinct roles for integrin splice variants in heart function and embryonic development. *Genes Dev.* 1998;12:1202–1216. doi: 10.1101/gad.12.8.1202
15. Martin PT, Kaufman SJ, Kramer RH, Sanes JR. Synaptic integrins in developing, adult, and mutant muscle: selective association of alpha1, alpha7A, and alpha7B integrins with the neuromuscular junction. *Dev Biol.* 1996;174:125–139. doi: 10.1006/dbio.1996.0057
16. Yin H, Price F, Rudnicki MA. Satellite cells and the muscle stem cell niche. *Physiol Rev.* 2013;93:23–67. doi: 10.1152/physrev.00043.2011
17. Dumont NA, Bentzinger CF, Sincennes MC, Rudnicki MA. Satellite cells and skeletal muscle regeneration. *Compr Physiol.* 2015;5:1027–1059. doi: 10.1002/cphy.c140068
18. Ziober BL, Chen Y, Kramer RH. The laminin-binding activity of the alpha 7 integrin receptor is defined by developmentally regulated splicing in the extracellular domain. *Mol Biol Cell.* 1997;8:1723–1734. doi: 10.1091/mbc.8.9.1723
19. Leung E, Lim SP, Berg R, Yang Y, Ni J, Wang SX, Krissansen GW. A novel extracellular domain variant of the human integrin α7 subunit generated by alternative intron splicing. *Biochem Biophys Res Commun.* 1998;243:317–325. doi: 10.1006/bbrc.1998.8092

20. Song WK, Wang W, Sato H, Bielser DA, Kaufman SJ. Expression of α7 integrin cytoplasmic domains during skeletal muscle development: alternate forms, conformational change, and homologies with serine/threonine kinases and tyrosine phosphatases. *J Cell Sci.* 1993;4:1139–1152. doi: 10.1242/jcs.106.4.1139
21. Velling T, Collo G, Sorokin L, Durbeej M, Zhang H, Gullberg D. Distinct α(7A)β1 and α(7B)β1 integrin expression patterns during mouse development: α(7A) is restricted to skeletal muscle but α(7B) is expressed in striated muscle, vasculature, and nervous system. *Dev Dyn.* 1996;207:355–371. doi: 10.1002/(SICI)1097-0177(199612)207:4<355::AID-AJA1>3.0.CO;2-G
22. Von Der Mark H, Williams I, Wendler O, Sorokin L, Von Der Mark K, Pöschl E. Alternative splice variants of alpha 7 beta 1 integrin selectively recognize different laminin isoforms. *J Biol Chem.* 2002;277:6012–6016. doi: 10.1074/jbc.M102188200
23. Hierck BP, Poelmann RE, Van Iperen L, Brouwer A, Gittenberger-de Groot AC. Differential expression of α6 and other subunits of laminin binding integrins during development of the murine heart. *Dev Dyn.* 1996;206:100–111. doi: 10.1002/(SICI)1097-0177(199605)206:1<100::AID-AJA9>3.0.CO;2-M
24. Van Der Flier A, Gaspar AC, Thorsteinsdóttir S, Baudoin C, Groeneveld E, Mummery CL, Sonnenberg A. Spatial and temporal expression of the β1D integrin during mouse development. *Dev Dyn.* 1997;210:472–486. doi: 10.1002/(SICI)1097-0177(199712)210:4<472::AID-AJA10>3.0.CO;2-9
25. Brancaccio M, Cabodi S, Belkin AM, Collo G, Koteliansky VE, Tomatis D, Altruda F, Silengo L, Tarone G. Differential onset of expression of α7 and β1D integrins during mouse heart and skeletal muscle development. *Cell Commun Adhes.* 1998;5:193–205. doi: 10.3109/15419069809040291
26. Hayashi YK, Chou FL, Engvall E, Ogawa M, Matsuda C, Hirabayashi S, Yokochi K, Ziober BL, Kramer RH, Kaufman SJ, et al. Mutations in the integrin alpha7 gene cause congenital myopathy. *Nat Genet.* 1998;19:94–97. doi: 10.1038/ng0598-94
27. Mayer U, Saher G, Fässler R, Bornermann A, Echtermeyer F, von der Mark H, Miosge N, Pöschl E, von der Mark K. Absence of integrin alpha7 causes a novel form of muscular dystrophy. *Nat Genet.* 1997;15:57–61.
28. Pegoraro E, Cepollaro F, Prandini P, Marin A, Fanin M, Trevisan CP, El-Messlemani AH, Tarone G, Engvall E, Hoffman EP, et al. Integrin α7β1 in muscular dystrophy/myopathy of unknown etiology. *Am J Pathol.* 2002;160:2135–2143. doi: 10.1016/S0002-9440(10)61162-5
29. Esposito T, Sampaolo S, Limongelli G, Varone A, Formicola D, Diodato D, Farina O, Napolitano F, Pacileo G, Gianfrancesco F, et al. Digenic mutational inheritance of the integrin alpha 7 and the myosin heavy chain 7B genes causes congenital myopathy with left ventricular non-compact cardiomyopathy. *Orphanet J Rare Dis.* 2013;8:1–13. doi: 10.1186/1750-1172-8-91
30. Xia W, Ni Z, Zhang Z, Sang H, Liu H, Chen Z, Jiang L, Yin C, Huang J, Li L, et al. Case report: a boy from a consanguineous family diagnosed with congenital muscular dystrophy caused by integrin alpha 7 (ITGA7) mutation. *Front Genet.* 2021;12:1–7. doi: 10.3389/fgene.2021.706823
31. Lopez MA, Mayer U, Hwang W, Taylor T, Hashmi MA, Jannapureddy SR, Boriek AM. Force transmission, compliance, and viscoelasticity are altered in the α7-integrin-null mouse diaphragm. *Am J Physiol - Cell Physiol.* 2005;288:282–289. doi: 10.1152/ajpcell.00362.2003
32. Kaplan JC, Hamroun D. The 2016 version of the gene table of monogenic neuromuscular disorders (nuclear genome). *Neuromuscul Disord.* 2015;25:991–1020. doi: 10.1016/j.nmd.2015.10.010
33. Flintoff-Dye NL, Welser J, Rooney J, Scowen P, Tamowski S, Hatten W, Burkin DJ. Role for the α7β1 integrin in vascular development and integrity. *Dev Dyn.* 2005;234:11–21. doi: 10.1002/dvdy.20462
34. Warrier S, Ramamurthy G, Eckert RL, Nikolaev VO, Lohse MJ, Harvey RD. cAMP microdomains and L-type Ca2+ channel regulation in Guinea-pig ventricular myocytes. *J Physiol.* 2007;580:765–776. doi: 10.1113/jphysiol.2006.124891
35. Kim MJ, Lim JE, Oh B. Validation of non-invasive method for electrocardiogram recording in mouse using Lead II. *Biomed Sci Lett.* 2015;21:135–143. doi: 10.15616/BSL.2015.21.3.135
36. Lindsey ML, Kassiri Z, Virag JAI, De Castro Brás LE, Scherrer-Crosbie M. Guidelines for measuring cardiac physiology in mice. *Am J Physiol Heart Circ Physiol.* 2018;314:H733–H752. doi: 10.1152/ajpheart.00339.2017
37. Severs NJ, Bruce AF, Dupont E, Rothery S. Remodelling of gap junctions and connexin expression in diseased myocardium. *Cardiovasc Res.* 2008;80:9–19. doi: 10.1093/cvr/cvn133
38. Palatinus JA, Rhett JM, Gourdie RG. The connexin43 carboxyl terminus and cardiac gap junction organization. *Biochim Biophys Acta - Biomembr.* 2012;1818:1831–1843. doi: 10.1016/j.bbamem.2011.08.006
39. Sedmera D, Gourdie RG. Why do we have Purkinje fibers deep in our heart? *Physiol Res.* 2014;63:9–18.
40. Michela P, Velia V, Aldo P, Ada P. Role of connexin 43 in cardiovascular diseases. *Eur J Pharmacol.* 2015;768:71–76. doi: 10.1016/j.ejphar.2015.10.030
41. Gutstein DE, Morley GE, Vaidya D, Liu F, Chen FL, Stuhlmann H, Fishman GI. Heterogeneous expression of gap junction channels in the heart leads to conduction defects and ventricular dysfunction. *Circulation.* 2001;104:1194–1199. doi: 10.1161/hc3601.093990
42. Patrick Gonzalez J, Ramachandran J, Xie LH, Contreras JE, Fraidenraich D. Selective Connexin43 inhibition prevents isoproterenol-induced arrhythmias and lethality in muscular dystrophy mice. *Sci Rep.* 2015;5:1–12. doi: 10.1038/srep15315
43. Himelman E, Lillo MA, Nouet J, Patrick Gonzalez J, Zhao Q, Xie LH, Li H, Liu T, Wehrens XHT, Lampe PD, et al. Prevention of connexin-43 remodeling protects against Duchenne muscular dystrophy cardiomyopathy. *J Clin Invest.* 2020;130:1713–1727. doi: 10.1172/JCI128190
44. Teunissen BEJ, Jongsma HJ, Bierhuizen MFA. Regulation of myocardial connexins during hypertrophic remodelling. *Eur Heart J.* 2004;25:1979–1989. doi: 10.1016/j.ehj.2004.08.007
45. Grant AO. Cardiac ion channels. *Circ Arrhythmia Electrophysiol.* 2009;2:185–194. doi: 10.1161/CIRCEP.108.789081
46. Wang YG, Samarel AM, Lipsius SL. Laminin acts via β1 integrin signalling to alter cholinergic regulation of L-type Ca2+ current in cat atrial myocytes. *J Physiol.* 2000;526:57–68. doi: 10.1111/j.1469-7793.2000.t01-1-00057.x
47. Kwon MS, Park CS, Choi KR, Park CS, Ahnn J, Il KJ, Eom SH, Kaufman SJ, Song WK. Calreticulin couples calcium release and calcium influx in integrin-mediated calcium signaling. *Mol Biol Cell.* 2000;11:1433–1443. doi: 10.1091/mbc.11.4.1433
48. Okada H, Lai NC, Kawaraguchi Y, Liao P, Copps J, Sugano Y, Okada-Maeda S, Banerjee I, Schilling JM, Gingras AR, et al. Integrins protect cardiomyocytes from ischemia/reperfusion injury. *J Clin Invest.* 2013;123:4294–4308. doi: 10.1172/JCI64216

SUPPLEMENTAL MATERIAL

Table S1. Clinical features of individuals with *ITGA7* null mutations

	Family 1.II-4	Family 1.II-3	Family 2.II-4	Family 2.II-8	Family 2.II-7
Genetic variants	c.806_818del [p.S269fs]; c.806_818del [p.S269fs]	N/A	c.2357+1G>A [r.spl?]; c.2278-1G>A [r.spl?]	c.2357+1G>A [r.spl?] c.2278-1G>A [r.spl?]	c.2357+1G>A [r.spl?]c.2278-1G>A [r.spl?]
Age of symptom onset	Birth – isolated stridor due to vocal cord paresis 37y cardiac symptoms	37y	± 50y	± 45y	± 40y
Skeletal muscle involvement					
Limb weakness	Ankle dorsiflexion weakness(MRC4+/5)	None	Ankle dorsiflexion weakness(MRC4+/5)	Mild weakness of proximal and distal leg muscles	Unknown
Respiratory	Congenital vocal cord paresis Nocturnal hypoventilation and hypercapnia requiring BiPAP	Not known	Recurrent respiratory failure with hypercapnia eventually requiring BiPAP	Postoperative hypercapnic coma	Postoperative hypercapnic coma
Other	Scoliosis				
Creatine Kinase	539-1000IU/L	N/A	52 IU/L	N/A	N/A
EMG	Myopathic units	N/A	Myopathic units	N/A	N/A
Muscle biopsy	Fibre size variation with occasional scattered atrophic fibres and nuclear bags	N/A	Lobulated fibres, increased variation in fibre size and type 2 fibre atrophy	N/A	N/A
Muscle imaging	Lower limb MRI: Severe atrophy of the medial	N/A	Muscle USS: Hyperechogenicity and calcifications in various	N/A	N/A

	head of gastrocnemius muscles bilaterally		muscles and a hyperechogenic signal surrounding the central tendon attachment of the tibialis anterior muscles		
Cardiac involvement					
Symptoms	Palpitations	Palpitations	Severe ascites and dyspnea indicating right-sided heart failure	Not reported	Dyspnea, ascites, and pitting edema indicating right-sided heart failure
ECG	First degree heart block, intraventricular conduction delay left axis deviation, paroxysmal atrial flutter	First degree heart block, left bundle branch block	Left bundle branch block, atrial flutter, high-grade atrioventricular block necessitating DDDR pacemaker implantation	N/A	N/A
24Hr-Holter-ECG	Ventricular ectopy including triplets and runs of NSVT, intermittent episodes of Mobitz type 1 second degree AV block	Ventricular ectopy with episodes of bigeminy and trigeminy and salvos of NSVT	N/A	N/A	N/A
Echocardiography	Mild relative basal septal hypertrophy and a hypertrophied anterolateral papillary muscle.	Relative mild basal septal hypertrophy	Moderate tricuspid and pulmonary valve insufficiency, moderately enlarged right ventricle, grossly enlarged right and left atrium,	N/A	N/A

			decreased systolic ejection fraction		
Cardiac MRI	Localised LVH. Sub-endocardial late gadolinium enhancement in the basal inferolateral wall. Preserved LV systolic function.	Mild LVH. Patch of late gadolinium enhancement in the basal to mid-LV segments. Preserved LV systolic function.	N/A	N/A	N/A

LVH: left ventricular hypertrophy; NSVT: non-sustained ventricular tachycardia; LV, left ventricle; MRC, Medical Research Council; BiPAP, Bilevel Positive Airway Pressure; AV, Atrioventricular; USS, Ultrasound Scan; MRI, Magnetic Resonance Imaging; DDDR, Dual-chamber rate-modulated; N/A: Not available.

Figure S1. Representative chromatograms from *ITGA7* deficient patients

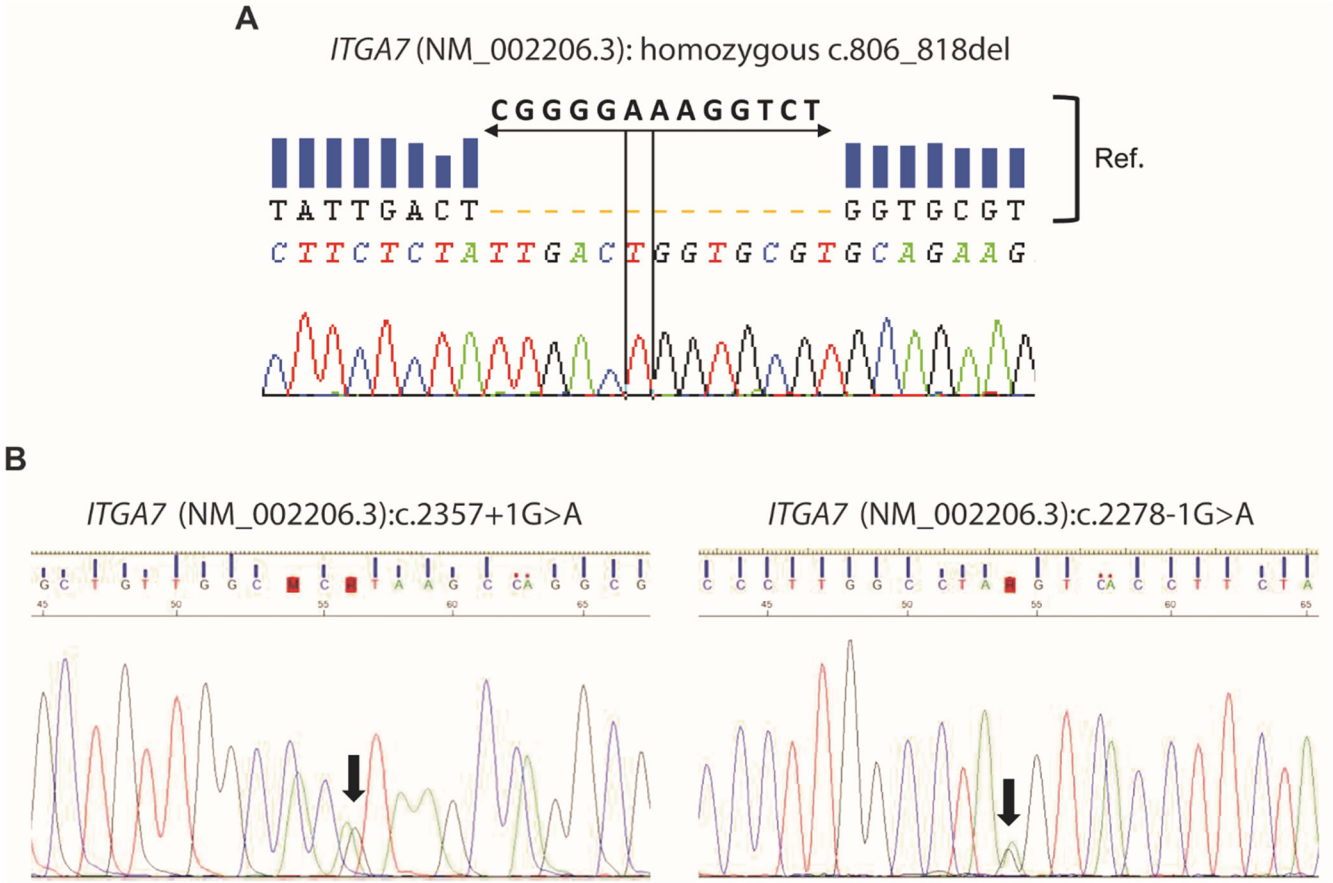

Representative chromatogram from the family 1 proband presenting homozygous c.806_818del deletion (**A**), line arrow indicates the deleted region. Representative chromatogram from the family 2 proband presenting c.2357+1G>A (left panel) and c.2278-1G>A (right panel) mutations (**B**), arrows indicate the mutation. Ref., reference sequence.

Figure S2. Cardiac arrhythmias and cardiomyopthy in family 1 proband`s brother

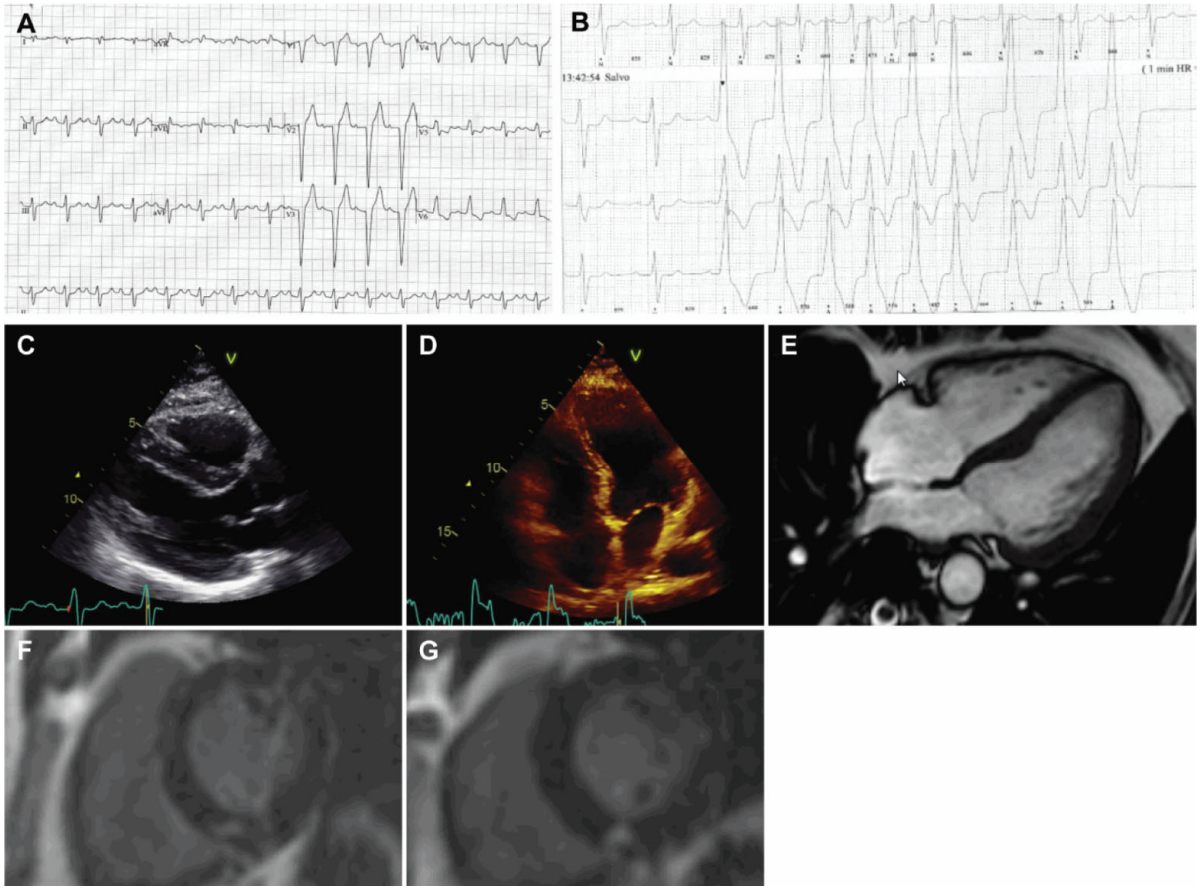

ECG, Holter, Echocardiography, and MRI images from the family 1 proband's brother (II:3). 12-lead ECG demonstrating first-degree heart block and left bundle branch block (LBBB) (**A**). 3-lead Holter analysis demonstrating broad-complex tachycardia consistent with non-sustained ventricular tachycardia (NSVT) (**B**). Parasternal long-axis view of the left ventricle showing a non-dilated LV (**C**). Apical 4-chamber view of the heart demonstrating no dilation with basal septal bulge (**D**). CMRI 4-chamber view demonstrating basal septal bulge and a non-dilated LV with no evidence of LVH elsewhere (**E**). CMRI late gadolinium enhancement sequences (**F,G**). ECG, Electrocardiography; MRI, Magnetic Resonance Imaging;CMRI, Cardiac Magnetic Resonance Imaging; LV, left ventricle; LVH, left ventricular hypertrophy..

Figure S3. Histological analysis of wild-type and *Itga7* $^{-/-}$ diaphragm and gastrocnemius muscles

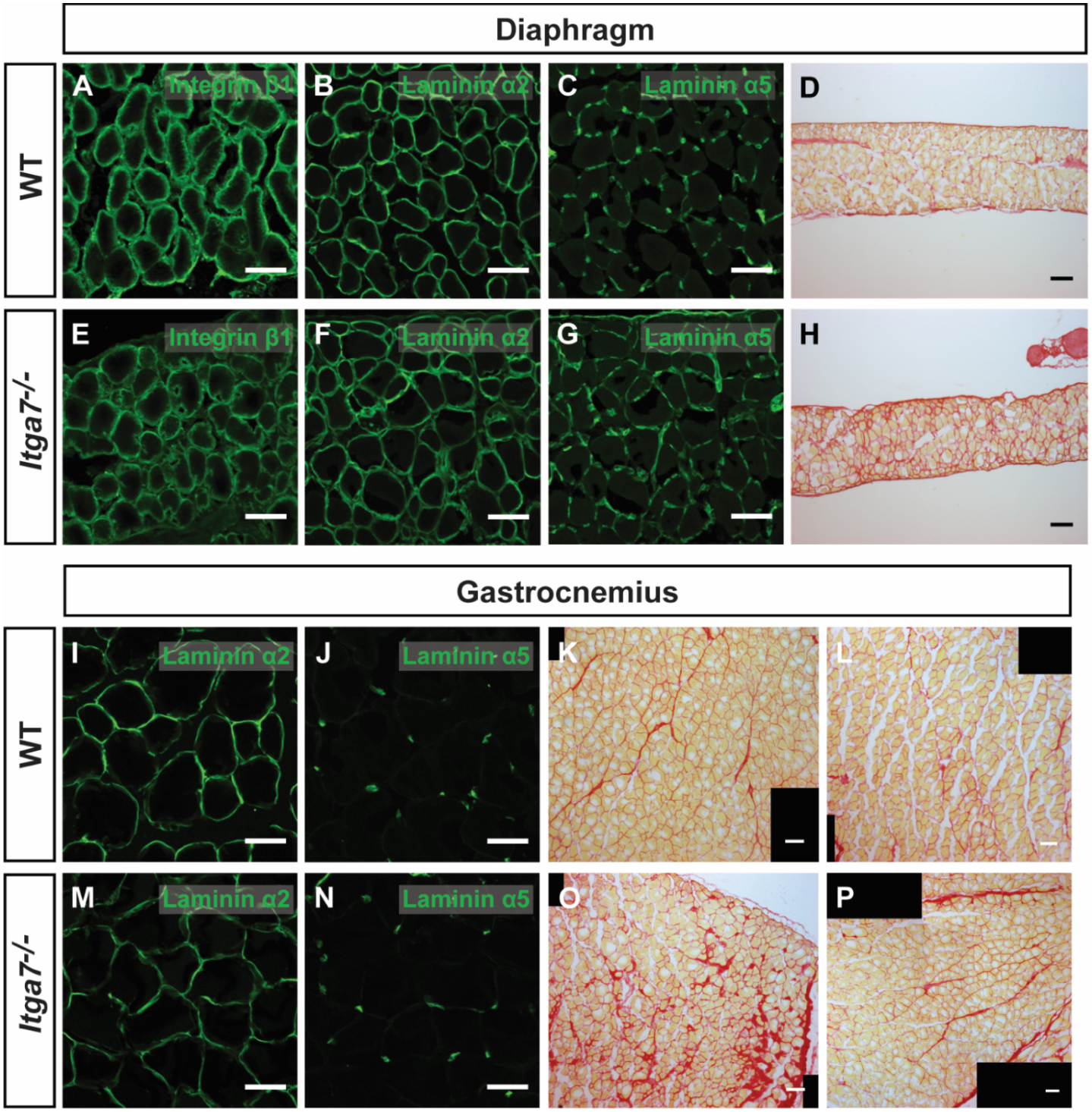

Transversal view of immunostaining for integrin β1D (**A, E**), laminin α2 (**B, F**), and laminin α5 (**C, G**) in WT (**A-C**) and *Itga7* $^{-/-}$ **(E-G**) diaphragm muscle. Integrin β1D staining is present in the fibre sarcolemma both in WT (**A**) and *Itga7*$^{-/-}$ diaphragm muscle (**E**), fluorescence intensity appears lower in *Itga7*$^{-/-}$ muscle. Laminin α2 immunostaining reveals normal laminin distribution in the fibre basal lamina in *Itga7* $^{-/-}$ muscle (**F**) when compared to WT muscle (**B**). Laminin α5 is detected in the endomysial vascular basal lamina in WT muscle (**C**), but in the absence of integrin α7, laminin α5 is additionally detected in the fibre basal lamina (**G**). Transversal view of Sirius Red staining in WT (**D**) and *Itga7*$^{-/-}$ (**H**) diaphragm muscle reveals an increase collagen accumulation in fibrotic tissue in *Itga7*$^{-/-}$ diaphragm muscle compared to WT diaphragm muscle. Laminin α2 is also detected in fibre basal lamina in the gastrocnemius muscle of WT (**I**) and *Itga7*$^{-/-}$ (**M**) mice, whereas laminin α5 is only detected in the endomysial vascular basal lamina in WT (**J**) and integrin α7 deficient mice (**N**). *Itga7*$^{-/-}$ gastrocnemius muscle exhibits regions of higher levels of collagen accumulation (**O**) compared to WT gastrocnemius muscle (**K, L**), but some areas with lower levels of collagen accumulation as well (**P**). Representative images of n=3 for each genotype. Scale bar: A-C, E-G, I, J, M, N= 50μm; D, H, K, L, O, P= 100μm. WT, wild-type.

Figure S4. Histological analysis of wild-type and *Itga7*$^{-/-}$ cardiac muscle

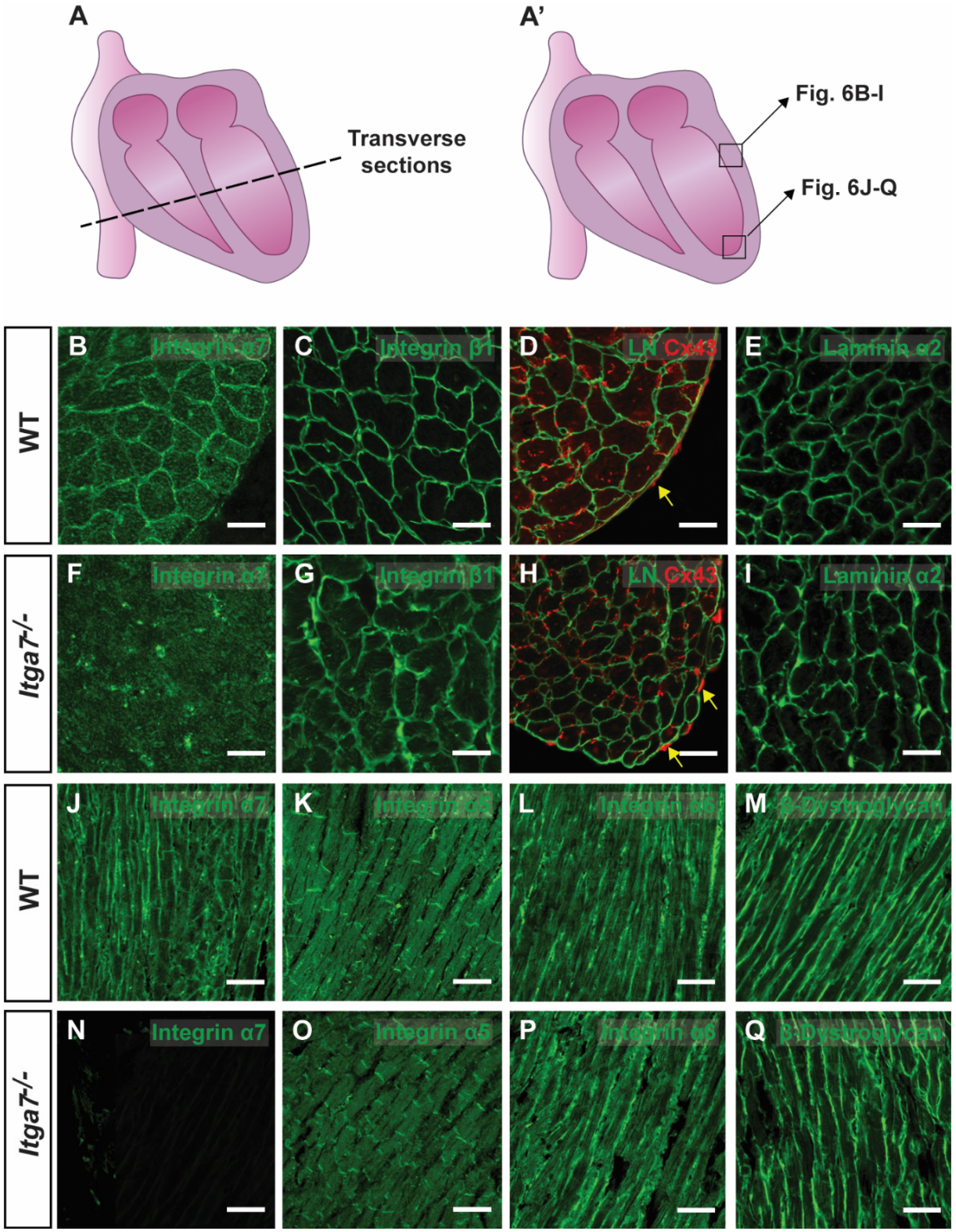

Schematic representation of transverse sections used for histological analysis of cardiac muscle (**A**) depicting the areas of analysis (**A'**). Transversal view of immunostaining for integrin α7B (**B, F**), integrin β1D (**C, G**), laminin (pan antibody) and connexin 43 (**D, H**) and laminin α2 (**E, I**) in the subendocardial area of WT (**B-E**) and *Itga7*$^{-/-}$ (**F-I**) cardiac muscle. Immunostaining for integrin α7B reveals the presence of integrin α7 in WT cardiac muscle (**B, J**) and its absence in *Itga7*$^{-/-}$ cardiac tissue (**F, N**), whereas integrin β1D staining is present in the cardiomyocyte basal lamina both in WT and *Itga7*$^{-/-}$ cardiac muscle (**C, G**). Total laminin and laminin α2 immunostaining reveals normal laminin distribution in the absence of integrin α7 (**D, E, H, I**). There is no considerable difference in connexin-43 distribution in the subendocardial layer in contact with the working myocardium in WT (**D**) and *Itga7*$^{-/-}$ (**H**) cardiac muscle. Longitudinal view of immunostaining for integrin α7 (**J, N**), integrin α5 (**K, O**), integrin α6 (**L, P**) and β-dystroglycan (**M, Q**) in the compact zone working myocardium of WT (**K-M**) and *Itga7*$^{-/-}$(**N-Q**) cardiac muscle. Immunostaining for integrin α5, α6 and β-dystroglycan reveals normal distribution in cardiomyocyte membrane in the absence of integrin α7 (**O-Q**). The yellow arrows indicate positive staining for connexin-43. LN, Laminin; Cx43, Connexin-43. Representative images of n=3 for each genotype. Scale bar: 25μm. WT, wild-type.

Figure S5. Integrin associated proteins talin and vinculin in wild-type and *Itga7*$^{-/-}$ diaphragm muscle

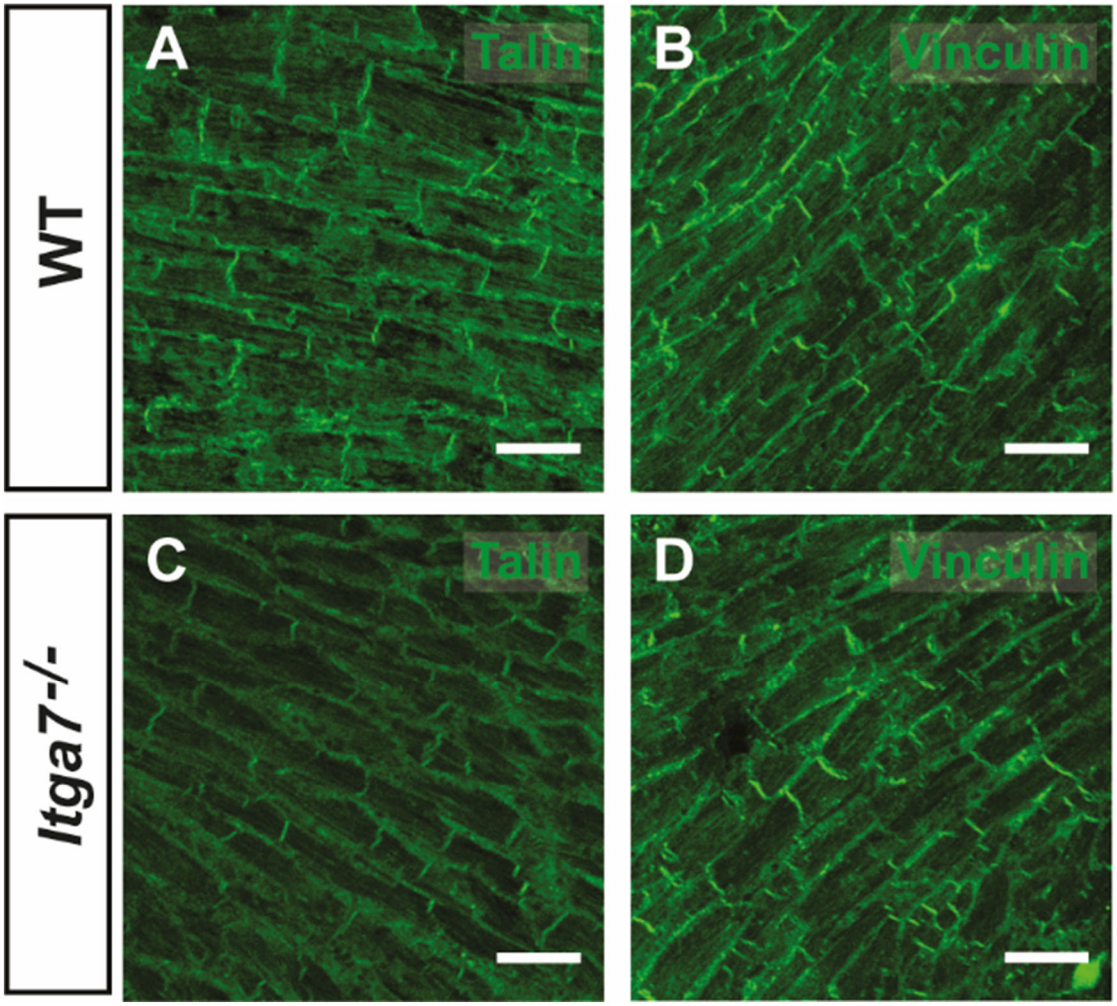

The distribution of talin (**A, C**) and vinculin (**B, D**) is not affected in *Itga7*$^{-/-}$ cardiac muscle (**C, D**) when compared to WT cardiac muscle (**A, B**). Representative images of n=3 for each genotype. Scale bar: 50μm. WT, wild-type.

Figure S6. Connexin-43 localization in guinea pig cardiomyocytes

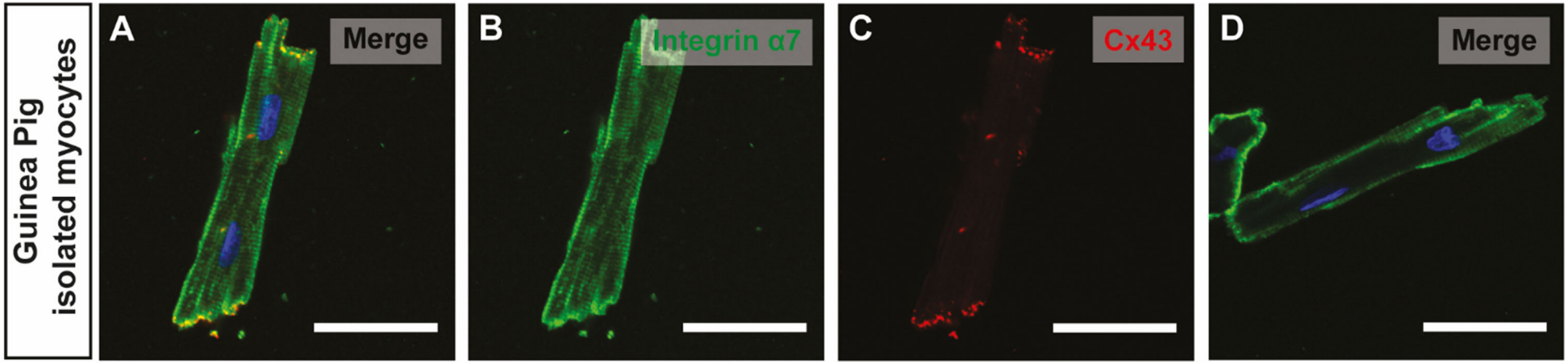

Integrin α7 (**B)**, connexin-43 (**C**) and integrin β1D (**D**) in adult isolated guinea pig cardiomyocytes. Integrin α7 and β1D are distributed along the cardiomyocyte membrane (**B, D**), and they co-localize with connexin-43 in the intercalated discs (**A**). DAPI (blue), integrin α7 (green) and connexin-43 (red). CX43, connexin-43. Representative images of n=3 for each genotype. Scale bar: 50μm.